Crossed-beam reaction of carbon atoms with hydrocarbon molecules. I. Chemical dynamics of the propargyl radical formation, C_3H_3 (X^2B_2), from reaction of $C(^3P_j)$ with ethylene, $C_2H_4(X^1A_g)$

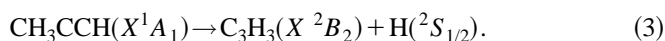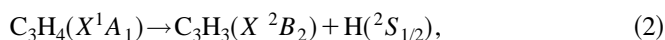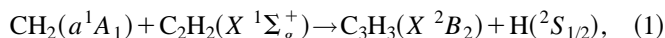R. I. Kaiser, Y. T. Lee,[a] and A. G. Suits[b]
Department of Chemistry, University of California, Berkeley, California 94720
and Chemical Sciences Division, Berkeley National Laboratory, Berkeley, California 94720

The reaction between ground-state carbon atoms, $C(^3P_j)$, and ethylene, $C_2H_4(X^1A_g)$, was studied at average collision energies of 17.1 and 38.3 kJmol^{-1} using the crossed molecular beams technique. Product angular distributions and time-of-flight spectra of $m/e=39$ were recorded. Forward-convolution fitting of the results yields a maximum energy release as well as angular distributions consistent with the formation of the propargyl radical in its X^2B_2 state. Reaction dynamics inferred from the experimental data indicate two microchannels, both initiated by attack of the carbon atom to the π-orbital of the ethylene molecule via a loose, reactant like transition state located at the centrifugal barrier. Following C_s symmetry on the ground state $^3A''$ surface, the initially formed triplet cyclopropylidene complex rotates in a plane roughly perpendicular to the total angular momentum vector around its C-axis, undergoes ring opening to triplet allene, and decomposes via hydrogen emission through a tight transition state to the propargyl radical. The initial and final orbital angular momenta **L** and **L**′ are weakly coupled and result in an isotropic center-of-mass angular distribution. A second microchannel arises from A-like rotations of the cyclopropylidene complex, followed by ring opening and H-atom elimination. In this case, a strong **L**-**L**′ correlation leads to a forward-scattered center-of-mass angular distribution. The explicit identification of C_3H_3 under single collision conditions represents a single, one-step mechanism to build up hydrocarbon radicals. Our findings strongly demand incorporation of distinct product isomers of carbon atom-neutral reactions in reaction networks simulating chemistry in combustion processes, the interstellar medium, as well as in outflows of carbon stars, and open the search for the hitherto unobserved interstellar propargyl radical. © 1996 American Institute of Physics. [S0021-9606(96)00639-3]

I. INTRODUCTION

The propargyl radical in its $^2B_2$ electronic ground state holds the global minimum on the C_3H_3 potential energy surface (PES) and has received considerable attention due to its potential importance in interstellar and planetary chemistry[1–2] and contribution to combustion processes.[3–7] High propargyl concentrations are predicted in oxygen rich hydrocarbon flames due to a partial delocalization of the unpaired B_2 electron and an inherent low reaction rate constant of $k(295 \text{ K})=5\times10^{-14}$ cm^3 s^{-1} with O_2.[8] Current combustion models postulate that soot formation and synthesis of polycyclic aromatic hydrocarbons (PAHs) are strongly correlated and initiated by recombination of two C_3H_3 radicals to C_6H_6 isomers [$k(295 \text{ K})=1.2\times10^{-10}$ cm^3 s^{-1}] followed by stepwise ring growth to larger PAHs.[9] However, little is known on the synthesis of the propargyl radical in hydrocarbon flames. Adamson investigated the reaction of singlet methylcarbene with acetylene, reaction (1), as a potential pathway,[10] whereas a unimolecular decomposition of vibrationally excited singlet allene or methylacetylene, C_3H_4 via C–H bond rupture, is suggested as a propargyl source, reactions (2) and (3)[11]

$$CH_2(a^1A_1) + C_2H_2(X\ ^1\Sigma_g^+) \rightarrow C_3H_3(X\ ^2B_2) + H(^2S_{1/2}), \quad (1)$$

$$C_3H_4(X^1A_1) \rightarrow C_3H_3(X\ ^2B_2) + H(^2S_{1/2}), \quad (2)$$

$$CH_3CCH(X^1A_1) \rightarrow C_3H_3(X\ ^2B_2) + H(^2S_{1/2}). \quad (3)$$

Besides its relevance in combustion chemistry, the propargyl isomer is expected to exist in interstellar and planetary environments. Its potential ethylene precursor has been widely incorporated into photochemical models of the stratosphere of Jupiter, Saturn, Uranus, Neptune, and Titan,[12] as well as into sophisticated ion-molecule networks of the Jovian ionosphere.[13] The very first detection of ethylene outside our solar system in circumstellar shells[14] fueled Herbst *et al.* to include the reaction of $C(^3P_j)$ with C_2H_4 in a generic chemical model of the circumstellar envelope surrounding IRC+10216, postulating the existence of C_3H_3 products.[15] Since the reaction network was based simply on spin-conservation and thermochemistry without investigation of the chemical dynamics, the explicit identification of any hitherto unobserved interstellar C_3H_3 isomer remains to be resolved, cf. Fig. 1.

Previous mechanistic information on the C/C_2H_4-system was derived from radioactive tracer studies of suprathermal $^{11}C(^3P_j)$ and $^{11}C(^1D_2)$ recoil atom reactions with $C_2H_4, C_2D_4, C_2H_4/O_2$, as well as C_2H_4/Ne-mixtures under
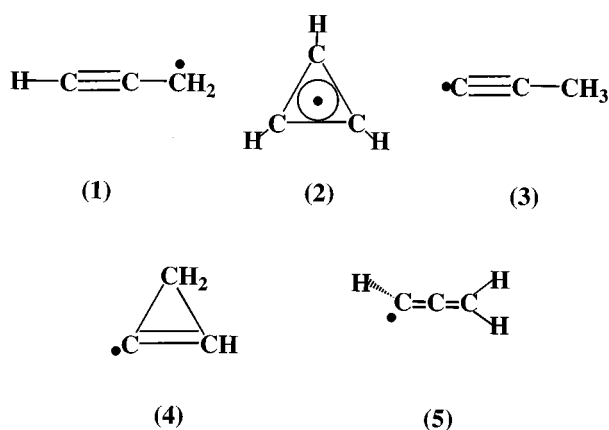
FIG. 1. Point groups, electronic ground states, and enthalpy of formations of C_3H_3 isomers relative to the propargyl radical: (1) propargyl (C_{2v}, $^2B_2$, 0 kJ mol^{-1}); (2) cyclopropen-1-yl (D_{3h}, $^2E''$, 100±25 kJ mol^{-1}); (3) propyn-1-yl (D_{3h}, ^2E, 147 kJ mol^{-1}); (4) cyclopropen-2-yl (C_s, $^2A'$, 233 kJ mol^{-1}); (5) allenyl (C_1, ^2A, 270 kJ mol^{-1}). Absolute enthalpy of formations of (1) and (2) were taken from Ref. 26.

bulk conditions.[16–25] Four product classes were identified: C_2H_2 (class 1), C_5H_x products (class 2), vinylacetylene (class 3), and allene/methylacetylene (class 4). Suprathermal $^{11}C(^1D_2)$ atoms add to the olefinic double bond to singlet cyclopropylidene (1, Fig. 2) followed by insertion between the previously joined carbon atoms to singlet allene (2). The vibrationally excited molecule could be stabilized via a third body collision, undergoes 1,3-hydrogen migration to methylacetylene (3) prior to its collisional deactivation, or is assumed to fragment to hydrogen and C_3H_3 radicals. To a minor amount, hot $^{11}C(^1D_2)$ inserts in a C–H bond to singlet vinylcarbene (4). Intermediate (4) undergoes 1,2- or 2,3-H migration to singlet allene (2), or methylacetylene (3), respectively, before a third body deactivation takes place. Thermal $^{11}C(^1D_2)$ atoms, however, are found to add exclusively to the ethylene π-bond.

Suprathermal $^{11}C(^3P_j)$ inserts into C–H bonds yielding triplet vinylcarbene (5) and adds to olefinic double bonds to triplet cyclopropylidene (6). The yield of C–H insertion products is reduced with increasing thermalization of the hot $^{11}C(^3P_j)$ atoms. Both triplet intermediates (5) and (6) are postulated to lose H to form C_3H_3 radicals with subsequent attack of a second ethylene molecule, producing 1-propyneyl-5 (7) and 1,2-pentadienyl-5 (8). Internally excited (7) and (8) abstract hydrogen atoms yielding 1-propyne (9) and 1,2-pentadiene (10). Vinylacetylene is assumed to be generated via reaction of C_2H_x radicals with ethylene molecules. The diminished concentration of vinylacetylene and acetylene goes hand in hand with a decreasing internal excitation of triplet C_3H_4 intermediates, suggesting C_2H_2 as a fragmentation product via C=C bond rupture in (5) or indirectly via vinylidenecarbene (11) after ring cleavage of (6) and 1,2-H-migration. Postulated cyclopropylidene intermediates were trapped as dimethyl-spiranes (12) as reaction products of carbon recoils with 2-butene.
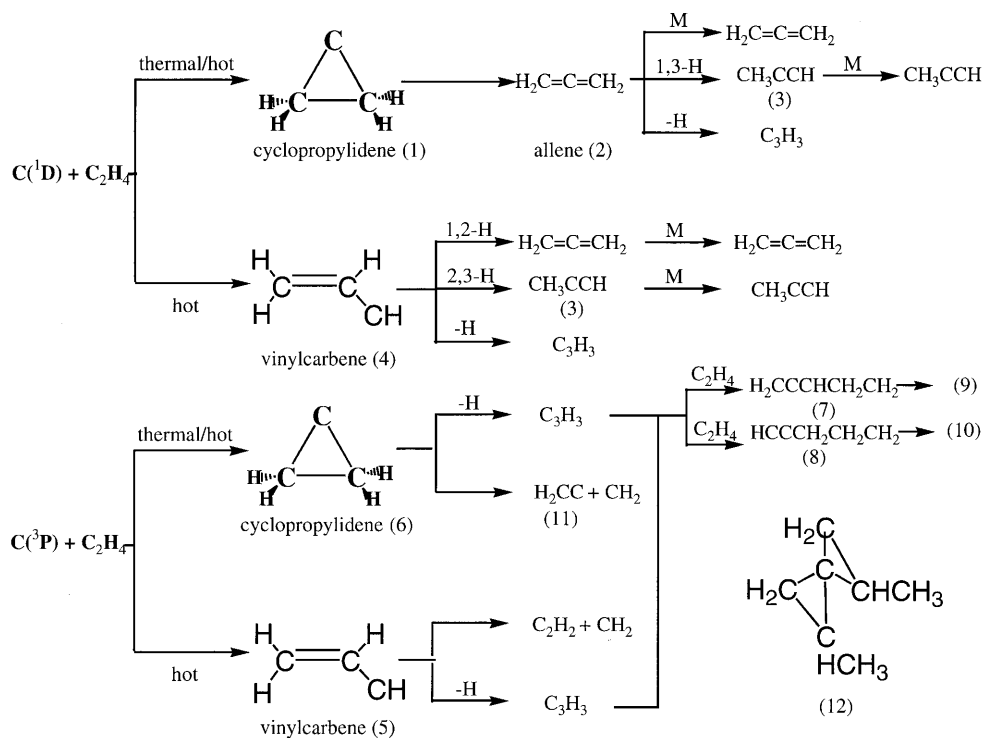
Here, we investigate the detailed chemical dynamics of

FIG. 2. Postulated reaction mechanisms and detected products in the C/C_2H_4 system as derived from bulk experiments of suprathermal $^{11}C(^3P_j)$ and $^{11}C(^1D_j)$ recoil atoms with C_2H_4, C_2D_4, C_2H_4/O_2, and C_2H_4/Ne mixtures.

TABLE I. Experimental beam conditions and 1σ errors: Most probable velocity v_0, speed ratio S, most probable relative collision energy with the ethylene molecules, E_{coll}, center-of-mass angle, θ_{CM}, composition of the carbon beam, and flux factor f_v in relative units, cf. Sec. IV A.

Beam	v_0, ms^{-1}	S	E_{coll}, kJ mol^{-1}	θ_{CM}	$C_1:C_2:C_3$	f_v
$C(^3P_j)$/Ne	1850 ± 30	4.5 ± 0.3	17.1 ± 0.7	45.3 ± 0.8	$1:0.6:1.8$	1.0
$C(^3P_j)$/He	2900 ± 80	4.0 ± 0.2	38.3 ± 2.1	34.1 ± 1.6	$1:0.2:0.3$	5.6 ± 1.1
C_2H_4	840 ± 40	8.3 ± 0.2	$\cdots$	$\cdots$	$\cdots$	$\cdots$

the atom-neutral reaction of $C(^3P_j)$ with $C_2H_4(X^1A_g)$ under single collision conditions at relative collision energies of 17.1 and 38.3 kJmol^{-1} as provided in crossed molecular beam experiments.[27] The detailed information on the reaction dynamics disclose the nature of the triplet C_3H_4 PES, the formation of C_3H_3 isomers in interstellar environments and hydrocarbon flames, reaction intermediates postulated in bulk experiments, and offer a valuable comparison to the $O(^3P_j)+C_2H_4(X^1A_g)$ reaction studied recently in our group.[28]

II. EXPERIMENT

The reactive scattering experiments are performed in a universal crossed molecular beam apparatus described in Ref. 29. A pulsed supersonic carbon beam was generated via laser ablation of graphite at 266 nm.[30] The 50/30 Hz, 35–40 mJ output of a Spectra Physics GCR-270-50/30 Nd:YAG laser is focused onto a rotating carbon rod. Ablated carbon atoms are seeded into neon (99.999%, Bay Area Gas) (experiment 1) or helium (99.999%, Bay Area Gas) (experiment 2) released by a Proch–Trickl pulsed valve operating at 100 Hz or 60 Hz, 80 μs pulses, and 4 atm backing pressure. A four slot chopper wheel mounted 40 mm after the ablation zone selects a 9.0/7.5 μs segment of the seeded carbon beam. Table I compiles the experimental beam conditions. The pulsed carbon beam and a continuous ethylene (99.99%, Matheson) beam with 584 ± 10 Torr backing pressure pass through skimmers with apertures of 1.0 and 0.58 mm, and cross at 90° with divergences of 3.0° and 4.7° in the interaction region of the scattering chamber at relative collision energies of 17.1 and 38.3 kJmol^{-1}. The reactively scattered products were detected in the plane of the beams using a rotatable detector consisting of a Brink-type electron-impact ionizer,[31] quadrupole mass filter, and a Daly ion detector[32] at different laboratory angles between 5.0^0 and 60.0^0 with respect to the carbon beam in 2.5^0–5.0^0 steps. The velocity distribution of the products was determined using the time-of-flight (TOF) technique[33] choosing a channel width of 10 μs. Counting times ranged from 0.5–5 h, averaged over several angular scans. The velocity of the supersonic carbon beam was monitored frequently after taking the data for 2–4 angles and minor velocity drifts corrected by adjusting the laser pulse delay within ±1 μs.[30] Reference angles were chosen at 35^0 and 47.5^0, respectively, to calibrate fluctuating carbon beam intensities and mass dial settings at the quadrupole controller.

III. DATA ANALYSIS

A. Velocity and speed ratio of the parent beams

The velocity distribution of each supersonic parent beam is defined by

$$N(v) = v_0^2 \exp\left(-\left(\frac{v_0}{\alpha} - S \right)^2 \right), \quad (4)$$

with the velocity v_0, the speed ratio S, and $\alpha = m/2RT$, mass of the molecule (atom) m, the temperature of the beam T and the ideal gas constant R. A transformation from the velocity to time domain yields

$$N(t) = \frac{L^3}{t^4} \exp\left(-\left(\frac{L}{\alpha t} - S \right)^2 \right), \quad (5)$$

where L is the neutral flight length. The most probable velocity and speed ratio are fitted after convolution over the ionizer length and the shutter function of the chopper wheel (Table I).

B. TOF spectra and laboratory angular distribution

Information on the velocity and angular distributions of products in the center-of-mass coordinate system was obtained by fitting the TOF spectra and the product angular distribution in the laboratory frame using a forward-convolution routine.[34,35] This iterative approach initially guesses the angular flux distribution $T(\theta)$ and the translational energy flux distribution $P(E_T)$ in the center-of-mass system (CM) which are assumed to be independent of each other. Since neither of the reactants is polarized, the cylindrical symmetry of the scattering process around the relative velocity vector in the CM-system restricts the angular dependence to θ, the scattering angle in the center-of-mass coordinate system measured from the direction of the carbon beam. The $P(E_T)$ is chosen as a parameterized function

$$P(E_T) = (E_T - B)^p \times (E_{av} - E_T)^q. \quad (6)$$

The B-parameter is related to the exit barrier with $B=0$ for a simple bond rupture without an exit-barrier. Peaking at a finite value E_P and for $B\neq0$, the first argument in Eq. (6) governs the energy difference of E_P and the low energy tail where $E_T\rightarrow0$, whereas the second argument describes a decaying function from E_P to the high energy tail. Likewise, $T(\theta)$ is defined as a sum of up to five Legendre-polynomials $P_1(\cos\theta)$ with coefficients a_1

$$T(\theta) = \sum_{l=0}^{5} a_l \times P_l(\cos \theta). \qquad (7)$$

Laboratory TOF spectra and the laboratory angular distribution (LAB) were calculated from the $T(\theta)$ and $P(E_T)$ distributions, and averaged over a grid of Newton diagrams defining the velocity and angular spread of each beam, detector acceptance angle, and the ionizer length. Best fits were obtained by iteratively refining the Legendre-coefficients and adjustable $P(E_T)$ parameters.

Collision energy dependent relative cross sections are computed by integrating $T(\theta)$ and $P(E_T)$:

$$\sigma'(E) = \int_0^\infty \int_0^{2\pi} \int_0^\pi P(E_T) T(\theta) \sin \theta \, d\theta \, d\varphi \, dE_T. \qquad (8)$$

Since the product yield under single collision conditions follows Eq. (9) with the number density of the ith reactant n_i and the relative velocity v_r, σ' has to be scaled by the flux factor f_v (Table I):

$$dn_p/dt = \sigma \times n(C) \times n(C_2H_4) \times v_r = \sigma' \times f_v. \qquad (9)$$

IV. RESULTS AND ANALYSIS

A. Reactive scattering signal

Reactive scattering signal was only observed at $m/e = 39$, i.e., C_3H_3. TOF spectra of $m/e = 36-38$ were recorded at several laboratory angles, but depict identical patterns with decreasing intensity. Therefore, the signal at $m/e = 36-38$ originates in cracking of the C_3H_3 parent in the ionizer, and channel 6–15 are not observed within detection limits (Table II). In addition, no radiative association to C_3H_4 ($m/e = 40$) or higher masses were detected. Endothermic channels 12–16 could not be opened at relative collision energies up to 38.3 kJmol^{-1} employed in the present experiments.

The detection of reactive scattering products C_2H_2, C_2H, and C_2 (channel 17–19) suffers from the inherent high background level at these masses arising from fragmentation of C_2H_4 in the detector. Attempts were made to identify these channels by replacing the continuous C_2H_4 source by a second pulsed valve with 0.25 mm nozzle diameter operating at 30 Hz with 1 atm backing pressure and increasing the pumping speed in the main chamber. Nevertheless, no reactive scattering signal was observed at $m/e = 26, 25, 24, 16$, or 15. Upper limits of 60% (channel 17) and 25% (channel 18) and 3% (channel 19) relative to $m/e = 39$ signal were derived.

B. Laboratory angular distribution (LAB) and TOF spectra

The most probable Newton diagrams of the reaction $C(^3P_j) + C_2H_4(X\,^1A_g) \rightarrow C_3H_3 + H$ and the laboratory angular distributions of the C_3H_3 product are displayed in Figs. 3 and 4 at collision energies of 17.1 and 38.3 kJmol^{-1}, respectively; TOF spectra are presented in Figs. 5 and 6. Both LAB distributions are very broad, and products are spread at least over a range of 50^0 in the scattering plane suggesting a large average translational energy release. Comparison of this scattering range with limiting circles which correspond to the

TABLE II. Thermochemistry of the reaction $C(^3P_j) + C_2H_4(X\,^1A_g)$. Enthalpies of formations were taken from Refs. 26, 36–38 (channels 12–13). The designation of the C_3H_3 isomers (channels 1–5) follows Fig. 1. C_3H_2 isomers (channels 6–11) are cyclopropenylidene (c-C_3H_2), propargylene (HCCCH), and vinylidenecarbene (CCCH$_2$).

#	Exit channel	Reaction enthalpy at 0 K, $\Delta_R H(0\ K)$, kJ mol^{-1}
1	$H_2CCCH(X\,^2B_2) + H(^2S_{1/2})$	-215.5 ± 8.4
2	c-$C_3H_3(X\,^2E'') + H(^2S_{1/2})$	-115 ± 25
3	$CCCH_3(X\,^2E) + H(^2S_{1/2})$	-69 ± 10
4	c'-$C_3H_3(X\,^2A') + H(^2S_{1/2})$	$+17 \pm 23$
5	$HCCCH_2(X\,^2A_1) + H(^2S_{1/2})$	$+56 \pm 25$
6	c-$C_3H_2(X\,^1A_1) + H_2(X\,^1\Sigma_g^+)$	-284.2 ± 10
7	$HCCCH(X\,^3B) + H_2(X\,^1\Sigma_g^+)$	-222 ± 20
8	$CCCH_2(X\,^1A_1) + H_2(X\,^1\Sigma_g^+)$	-194 ± 10
9	$HCCCH(a\,^1A_1) + H_2(X\,^1\Sigma_g^+)$	-157 ± 25
10	c-$C_3H_2(a\,^3A_1) + H_2(X\,^1\Sigma_g^+)$	-67 ± 10
11	$CCCH_2(a\,^3B_1) + H_2(X\,^1\Sigma_g^+)$	-46 ± 10
12	l-$C_3H(X\,^2\Pi_{1/2}) + H(^2S_{1/2}) + H_2(X\,^1\Sigma_g^+)$	$+154 \pm 15$
13	c-$C_3H(X\,^2B_2) + H(^2S_{1/2}) + H_2(X\,^1\Sigma_g^+)$	$+143.8 \pm 15$
14	$C_3(X\,^1\Sigma_g^+) + 2H_2(X\,^1\Sigma_g^+)$	$+39.3 \pm 0.5$
15	$C_3(a\,^3\Pi_u) + 2H_2(X\,^1\Sigma_g^+)$	$+241.3 \pm 0.5$
16	$C_2H_3(X\,^2A') + CH(X\,^2\Pi_j)$	$+118.5$
17	$C_2H_2(X\,^1\Sigma_g^+) + CH_2(X\,^3B_2)$	-159
18	$C_2H(X\,^2\Sigma^+) + CH_3(X\,^2A_2'')$	-60 ± 4
19	$C_2(X\,^1\Sigma_g^+) + CH_4(X\,^1A_1)$	-9.8

maximum energy release of different C_3H_3 isomers confine energetically accessible products to the propargyl, cyclopropen-1-yl, or propyn-1-yl isomer. Cyclopropen-2-yl can most likely be eliminated, since its observable range is restricted between $\approx 42-47^0$ at lower, and $\approx 15-45^0$ at higher collision energies. Reactive scattering signal, however, extends to at least $12.5-60.0^0$ and $10-55^0$, respectively. Contributions from the velocity spread of the carbon beam (Table I) can hardly account for this discrepancy. The allenyl isomer is energetically inaccessible at both collision energies and is excluded from the discussion.

C. Center-of-mass translational energy distribution, $P(E_T)$

The translational energy distributions in the center-of-mass-frame $P(E_T)$ are presented together with the center-of-mass angular distributions $T(\theta)$ in Figs. 7–8. Best fits of TOF spectra and LAB distributions were achieved with $P(E_T)s$ extending to $E_{max} = 230$ and 255 kJmol^{-1}, respectively. The fits are relatively insensitive to the q-parameter (Sec. II B): Adding or cutting the high energy tail by ± 20 kJmol^{-1} did not affect the calculated data due to the limited signal to noise ratio and the unfavorable kinematic relation as well as the uncertainty in the velocity spread of the carbon beam. The magnitude of E_{max} can be used to identify the nature of the product isomer if their energetics are well separated. Table III compiles the maximal translational energy release, i.e., the sum of the reaction exothermicity and relative collision energy, with the reasonable approximation of cold ethylene molecules in the supersonic expansion. The formation of the propargyl isomer is consistent with the ex-
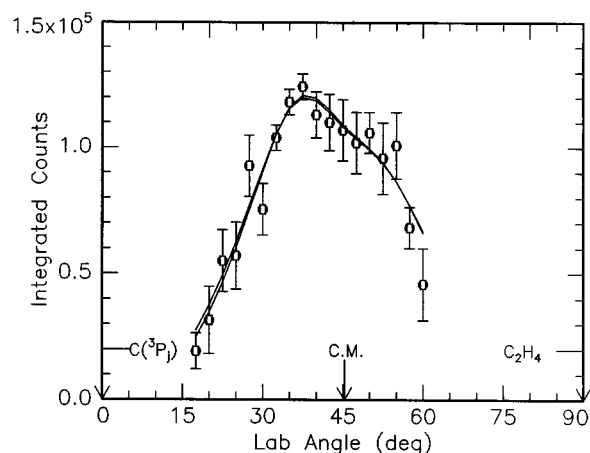
FIG. 3. Lower: Newton diagram for the reaction $C(^3P_j)+C_2H_4(X\ ^1A_g)$ at a collision energy of 17.1 kJ mol^{-1}. The circles stand for the maximum center-of-mass recoil velocity of different C_3H_3-isomers; from outer to inner: Propargyl, cyclopropen-1-yl, and propyn-1-yl. Upper: Laboratory angular distribution of product channel at $m/e=39$. Circles and 1σ error bars indicate experimental data, the solid lines the calculated distributions for the upper and lower carbon beam velocity (Table I). C.M. designates the center-of-mass angle. The solid lines point to distinct laboratory angles whose TOFs are shown in Fig. 5.
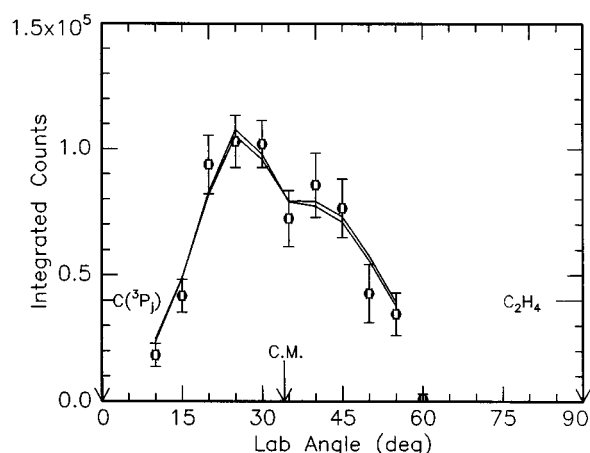
FIG. 4. Lower: Newton diagram for the reaction $C(^3P_j)+C_2H_4(X\ ^1A_g)$ at a collision energy of 38.3 kJ mol^{-1}. The circles stand for the maximum center-of-mass recoil velocity of different C_3H_3 isomers; from outer to inner: Propargyl, cyclopropen-1-yl, propyn-1-yl, and cyclopropen-2-yl. Upper: Laboratory angular distribution of product channel at $m/e=39$. Circles and 1σ error bars indicate experimental data, the solid lines the calculated distributions for the upper and lower carbon beam velocity (Table I). C.M. designates the center-of-mass angle. The solid lines point to distinct laboratory angles whose TOFs are shown in Fig. 6.

perimentally determined high energy cutoff. Even within the error limits, the 100 kJmol^{-1} less stable cyclopropenyl radical can be clearly dismissed (Fig. 1).

Besides identification of structural isomers, the most probable translational energy gives the order-of-magnitude of the barrier height in the exit channel. Both $P(E_T)s$ show a broad plateau between 28–43 kJmol^{-1}, nearly independent of the collision energy. These data clearly indicate a significant geometry as well as electron density change from the C_3H_4 complex to the products resulting in a repulsive bond rupture from a tight transition state. The existence of an exit potential energy barrier is further indicated by the large fraction of energy released into translational motion of the products, i.e., 31±3% and 42±3%, respectively.

D. Center-of-mass angular distribution, $T(\theta)$

Both $T(\theta)$s are weakly polarized and show an intensity ratio of $T(\theta)$ at $\theta=0°$ to 180° increasing from 1.7±0.1 to

2.0±0.1 as the collision energy rises. Since the total fraction f of forward-scattered signal with respect to the carbon beam slightly decreases from f (17.1 kJmol^{-1})=13±2% to f(38.3 kJmol^{-1})=8±2% with increasing collision energy, the shape of the $T(\theta)$s does not propose the existence of a conventional osculating C_3H_4 complex.[40,41] The results rather suggest two microchannels: A forward-scattered contribution with a strong correlation of the initial and final orbital angular momenta **L** and **L**$'$ perpendicular to the initial and final relative velocity vectors **v** and **v**$'$ (microchannel 1) and an isotropic channel, possibly symmetric around $\theta=\pi/2$ (microchannel 2), but governed by a weak **L** and **L**$'$ coupling allowing any of the four hydrogen atoms to depart, if the exit barriers are close together. Two alternative scenarios might account for a potential forward–backward symmetry of the center-of-mass angular distribution of microchannel 2. First, the decomposing C_4H_3 complex could hold a lifetime longer than its rotational period.[39–41] Second, a symmetric transition state might result in a center-of-mass angular distribution symmetric
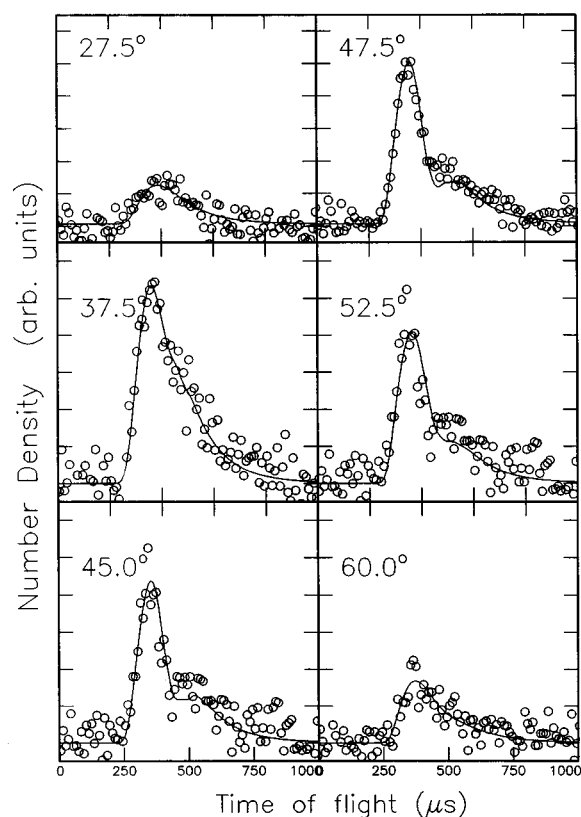
FIG. 5. Time-of-flight data at $m/e=39$ for laboratory angle 27.5, 37.5, 45.0, 47.5, 52.5, and 60.0° at a collision energy of 17.1 kJ mol^{-1}. Open circles represent experimental data, the solid line the fit. TOF spectra have been normalized to the relative intensity at each angle.

FIG. 6. Time-of-flight data at $m/e=39$ for laboratory angle 15.0, 20.0, 25.0, 35.0, 45.0, and 55.0° at a collision energy of 38.3 kJ mol^{-1}. Open circles represent experimental data, the solid line the fit. TOF spectra have been normalized to the relative intensity at each angle.
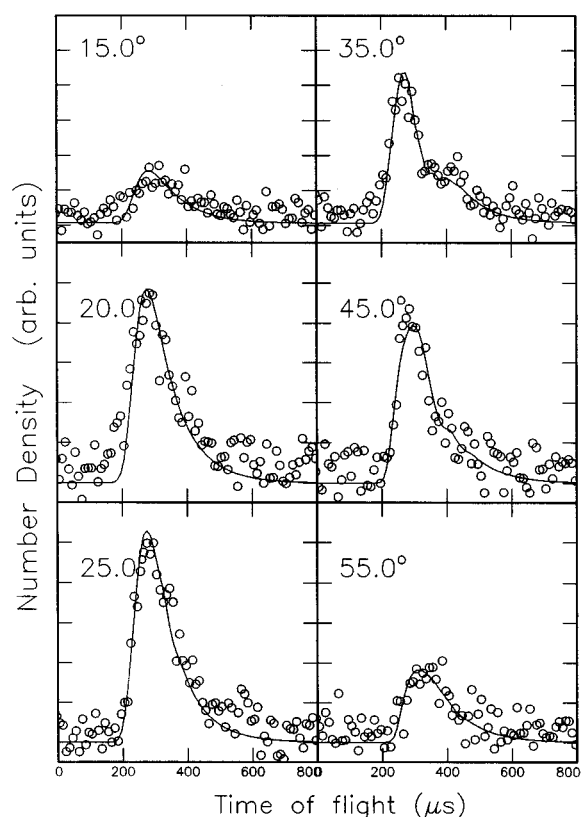
around $\pi/2$ despite a complex lifetime shorter than its rotational period since the hydrogen atom from either end can depart with equal probability in θ and $\pi-\theta$.

The weak polarization of microchannel 2 can be understood in terms of total angular momentum conservation and angular momentum disposal.[40–41] The total angular momentum $\mathbf{J}$ is given by

$$\mathbf{J}=\mathbf{L}+\mathbf{j}+\mathbf{j_n}=\mathbf{L}'+\mathbf{j}'+\mathbf{j}_n', \tag{10}$$

with the rotational angular momenta of the reactants and products $\mathbf{j}$ and $\mathbf{j}'$, as well as $\mathbf{j_n}$ and $\mathbf{j}_n'$ the initial and final nuclear momenta. In terms of a classical treatment and bearing in mind that $\mathbf{j_n}\ll\mathbf{L}$, $\mathbf{j_n}\ll\mathbf{j}$, $\mathbf{j}_n'\ll\mathbf{L}'$, and $\mathbf{j}_n'\ll\mathbf{j}'$, Eq. (10) reduces to Eq. (11)

$$\mathbf{J}=\mathbf{L}+\mathbf{j}=\mathbf{L}'+\mathbf{j}'. \tag{11}$$

A further simplification is introduced by comparing the magnitude of $\mathbf{L}$ and $\mathbf{j}$. Since bulk experiments indicate that the reaction of $C(^3P_j)$ with olefins and alkynes proceeds within orbiting limits[42] and our relative cross sections rise with decreasing collision energy (Sec. IV E), the maximum impact parameter b_{max} leading to a complex formation is approximated in terms of the classical capture theory to b_{max}(17.1 kJmol^{-1})=3.7 Å and b_{max}(38.3 kJmol^{-1})=3.2 Å (see Appendix A and Table IV). The maximum orbital angular momentum L_{max} relates to b_{max} via

$$L_{max}=\mu \, b_{max}v_r, \tag{12}$$

where μ is the reduced mass and v_r the relative velocity of the reactants: Thus L_{max}(17.1 kJmol^{-1})=99$\hbar$ and L_{max}(38.3 kJmol^{-1})=128$\hbar$. Since C_2H_4 is produced in a supersonic expansion and j peaks at only 3$\hbar$ at a typical rotational temperature of 30 K, $\mathbf{j}$ contributes less than 3% to the total angular momentum, and $\mathbf{J}$ becomes the initial orbital angular momentum $\mathbf{L}$

$$\mathbf{L}\approx\mathbf{J}=\mathbf{L}'+\mathbf{j}'. \tag{13}$$

Further, an upper limit of L' can be estimated by assuming a relative velocity of the recoiling products corresponding to the average translational energy release $\langle E_T\rangle$, and choosing an acetylenic C≡C bond length of 1.08 Å as the exit impact parameter to L'(17.1 kJmol^{-1})=20$\hbar$ and L'(38.3 kJmol^{-1})=24$\hbar$. Since $L'\approx0.2$ L, $\mathbf{L}$ and $\mathbf{L}'$ are not likely to be strongly coupled on average, resulting in weakly polarized $T(\theta)$s. This prevents us from classifying the decomposing complex as prolate- or oblate-like solely based on $T(\theta)$: In a prolate case, low M' values dominate, where M' denotes the projection of $\mathbf{J}$ on the decomposing complex' principal axis parallel to $\mathbf{v}'$, and the complex decomposes in the plane containing the relative velocity vector. An oblate decomposition geometry directs large M' values, and a fragmentation parallel to $\mathbf{J}$. Therefore, a sharply peaked $T(\theta)$ is
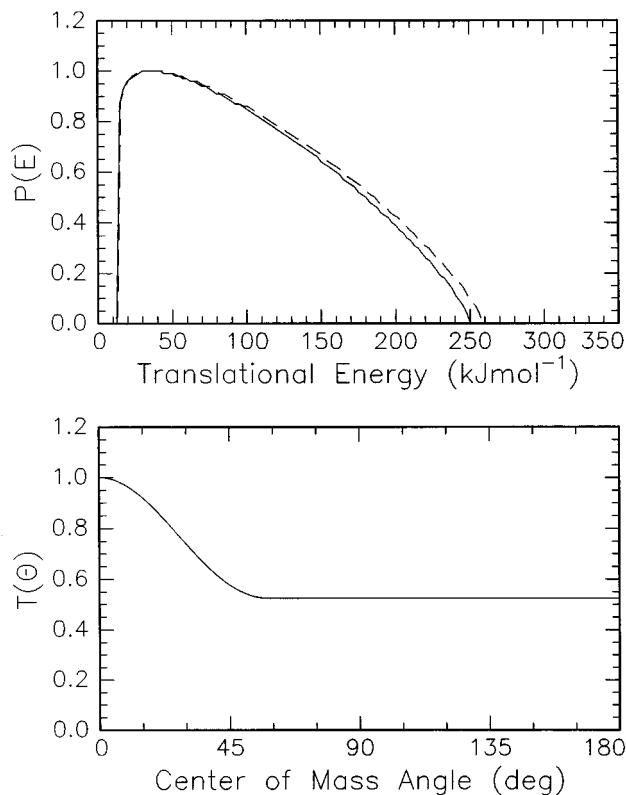
FIG. 7. Lower: Center-of-mass angular flux distribution for the reaction $C(^3P_j)+C_2H_4(X\ ^1A_g)$ at a collision energy of 17.1 kJ mol^{-1}. Upper: Center-of-mass translational energy flux distribution for the reaction $C(^3P_j)+C_2H_4(X\ ^1A_g)$ at a collision energy of 17.1 kJ mol^{-1}. Dashed and solid lines limit the range of acceptable fits within 1σ error bars.
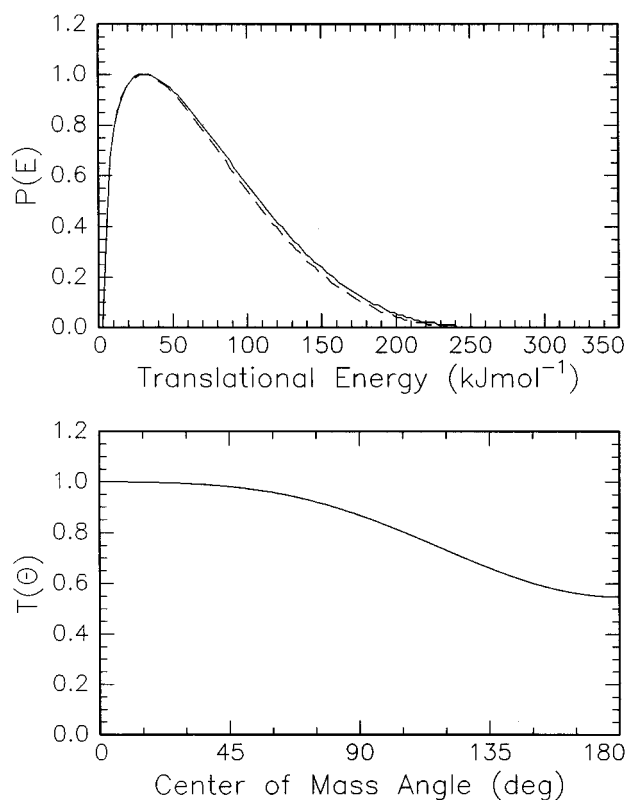
FIG. 8. Lower: Center-of-mass angular flux distribution for the reaction $C(^3P_j)+C_2H_4(X\ ^1A_g)$ at a collision energy of 38.3 kJ mol^{-1}. Upper: Center-of-mass translational energy flux distribution for the reaction $C(^3P_j)+C_2H_4(X\ ^1A_g)$ at a collision energy of 38.3 kJ mol^{-1}. Dashed and solid lines limit the range of acceptable fits within 1σ error bars.

expected only if **L** and **L**′ strongly correlated, i.e., parallel or antiparallel with $\mathbf{j}' \ll \mathbf{L}'$, or if M' is zero. This weak **L**−**L**′ correlation is a direct result of large impact parameters contributing to the complex formation and the inability of the departing H atom to carry significant orbital angular momentum supporting recent bulk experiments[42] and our findings of a long-range term dominated interaction potential.

E. Flux contour map and total relative cross section

The center-of-mass flux contour maps $I(\theta,E_T) \sim T(\theta) \times P(E_T)$ for both collision energies are shown in Figs. 9–10. As expected from discussed $T(\theta)$s, the product flux peaks in forward direction with respect to the carbon beam on the relative velocity vector. Integrating this flux distribution over θ, φ, E_T, and correcting for the reactant flux as well as relative reactant velocity, we find a total, relative cross section ratio of σ (17.1 kJmol^{-1})/σ(38.3 kJmol^{-1})=3.5±1.1. This ratio is most sensitive to the fragmentation applied for C_3, especially in the Ne seeded experiments where larger carbon clusters contribute ~80% to the carbon number density (Table I). Lowering the fragmentation pattern of C_3 by 30% reduces σ(17.1 kJmol^{-1})/σ(38.3 kJmol^{-1}) to 2.6±0.9. Nevertheless, the drop in the cross section with increasing collision energy is consistent with recent bulk experiments.[42] Clary et al. inves-

tigated reaction rate constants at 293 K of $C(^3P_j)$ atoms with alkynes as well as alkenes, indicating the reactions proceed fast ($k=10^{-10}-10^{-9}$ cm^3 s^{-1}) without entrance barrier within orbiting limits, i.e., the C–C$_2$H$_4$ interaction is dominated by a barrier-less, attractive long-range intermolecular dispersion forces giving rise to a loose, reactant-like transition state located at the centrifugal barrier to the triplet C$_3$H$_4$ PES. Taking L_{max} from Table IV, and Eq. (A6), we calculate the lower limit of barrier locations to R_{max} (17.1 kJmol^{-1})=3 Å and R_{max} (38.3 kJmol^{-1})=2.6 Å.

Simple capture calculations yield a cross section proportional to $E_{coll}^{-1/3}$ and $[\sigma$ (17.1 kJmol^{-1})/σ(38.3 kJmol^{-1})$]_{capture}$=1.3±0.1. This treatment assumes the reaction proceeds with unit efficiency after barrier-crossing and under absence of steric effects. However, at higher relative collision energies the orbiting radii become comparable or smaller than the van der Waals radii. Since the capture assumption is based solely on a long-range C_6 attraction, this approximation breaks down, and the structure of the molecule becomes important. Alternatively, the presence of a second reaction channel might contribute to this deviation. Equation (14) outlines this alternative for j exit channels with cross sections σ_i at two collision energies E_1 and E_2:

$$\left[\frac{\sigma(E_1)}{\sigma(E_2)}\right]_{capture} = \left[\frac{\sum_{i=1}^{j}\sigma_i(E_1)}{\sum_{i=1}^{j}\sigma_i(E_2)}\right]_{experiment} . \quad (14)$$

TABLE III. Comparison of the maximal available translational energy release, $E_{tot(theor)}$, of the reaction $C(^3P_j)+C_2H_4(X\ ^1A_g)\rightarrow C_3H_3+H(^2S_{1/2})$ for different C_3H_3 isomers with experimental data, $E_{tot(exp)}$.

E_{coll}, kJ mol^{-1}	Propargyl	Cyclopropen-1-yl	$E_{tot(theor)}$, kJ mol^{-1} Propyn-1-yl	Cyclopropen-2-yl	Allenyl	$E_{tot(exp)}$, kJ mol^{-1}
17.1	232±9	132±34	85±9	1±9	...	230±30
38.3	253±10	153±35	106±10	20±10	...	255±25

The framework of the capture theory cannot supply information on how many exit channels are involved and yields only a total cross section, here $\sigma(E_1)$ and $\sigma(E_2)$. Assuming a constant opacity function and an ideal, long range-term dominated potential, both sides in Eq. (14) are identical only if we find all $\sigma_i(E_1)$ and $\sigma_i(E_2)$ or if only one channel is involved ($j=1$). Therefore, our data might suggest the existence of at least a second channel leading to products with m/e ratios different from 39. Its relative cross section must increase with rising collision energy to reduce the right hand side of Eq. (14).

F. Energy partition of total available energy

The total available energy, E_{tot}, channels into product translation, E_{tr}, rotation, E_{rot}, and vibration, E_{vib}. E_{tr} can be obtained from the $P(E_T)s$ and, hence, equals $\langle E_T \rangle$, cf. Sec. IV C. Since the reaction products in the crossed beam experiment were identified as atomic hydrogen and the propargyl radical, the rotational energy is confined to the C_3H_3 isomer. The rotational constants $A=9.6081$ cm^{-1}, $B=0.317\ 57$ cm^{-1}, and $C=0.307\ 65$ cm^{-1} classify this radical as a highly prolate asymmetric top with asymmetry parameter $\kappa=-0.9978$.[43] Its energy levels follow therefore in good approximation those of a symmetric top

$$E=hc[BJ(J+1)+(A-B)K^2].\qquad(15)$$

J denotes the rotational quantum number of 79 ($E_{coll}=17.1$ kJmol^{-1}) and ~104 ($E_{coll}=38.3$ kJmol^{-1}) since the total angular momentum is conserved. K indicates the component of the rotational angular momentum about the principal axis, with $K=0$ for no rotation about the figure axis, but perpendicular to it, and $K\approx J$ for a fast rotation about the principal axis, with a slow end-over-end one.

Since no explicit information on the K-distribution is available, an exact solution of this problem is unrealizable. Here, we calculate first the rotational energy for $K=0$, and, therefore the maximal vibrational energy release E_{vib} in the propargyl product. This approach is referred to as ''low K approximation.'' Second, we assume the forward-peaking

microchannel 1 corresponds to rotations of the propargyl radical around its C_2 axis. Finally, the highest energetically accessible K states, K_{max}, are computed assuming no vibrational excitation of the C_3H_3. This gives us the upper limit of the average product rotational excitation and an order of magnitude of the lowest tilt angle α_{min} of the propargyl C_2 axis with respect to $\mathbf{j}'$ in terms of the classical vector model to

$$\alpha_{min}=\arccos(K_{max}/j').\qquad(16)$$

As evident from Table V, the low K approximation yields an increasing channeling of total energy into rotational degrees of freedom as the collision energy rises. The reduced fraction of vibrational energy from 59% to 43% indicating an incomplete energy randomization before the C_4H_3 complex decomposes, cf. Sec. V E. In case of zero vibrational excitation of the propargyl radical and upper K limit, the C_2 principal axis tilts about 68° on average with respect to $\mathbf{j}$ and clearly indicates a dominant end-over-end-rotation of the C_3H_3 radical. Even the assumption that microchannel 1 contributes solely to rotations around the propargyl figure axis is consistent with the energy conservation (Table V) as well as with a decreasing fraction of vibrational energy, in this case from 24% to 8%, as the relative collision energy rises.

V. DISCUSSION

The crossed beam method allows insight into the dynamics of the reaction and reveals unprecedented information on the reaction intermediate. In the following discussion, we outline all theoretically feasible reaction pathways on the C_3H_4 PES[43–58] to the propargyl radical without imposing any dynamic or energetic constraints (Sec. V B). Thereafter, the observed dynamics and energetics are compared to what is expected based on these ad-hoc pathways. Channels not compatible with the experimental results are eliminated. This approach ultimately identifies the remaining channel as the only possible one.

TABLE IV. Maximum impact parameter b_{max}, maximum initial orbital angular momentum, L_{max}, and capture cross sections σ at two relative collision energies E_{coll} employed in the present experiments. Cross sections σ are calculated for no [$P(b)=1$], one [$P(b)=2/3$], and two [$P(b)=1/3$] repulsing surfaces of the split triplet manifold.

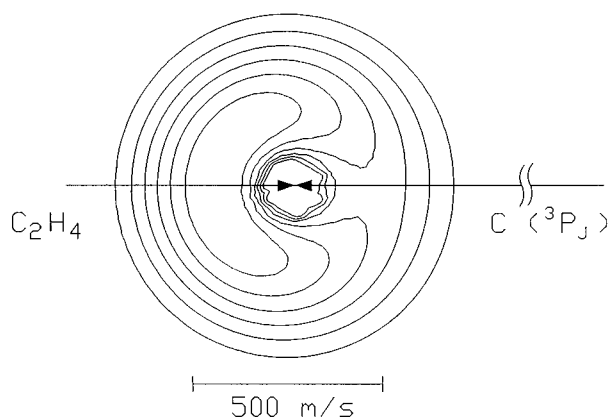| E_{coll}, kJ mol^{-1}	b_{max}, Å	L_{max}, $\hbar$	σ, Å^2 [$P(b)=1$]	σ, Å^2 [$P(b)=2/3$]	σ, Å^2 [$P(b)=1/3$]
17.1	3.7	99	42	28	14
38.3	3.2	128	32	21	11

FIG. 9. Contour flux map distribution for the reaction $C(^3P_j)+C_2H_4(X\ ^1A_g)$ at a collision energy of 17.1 kJ mol^{-1}.
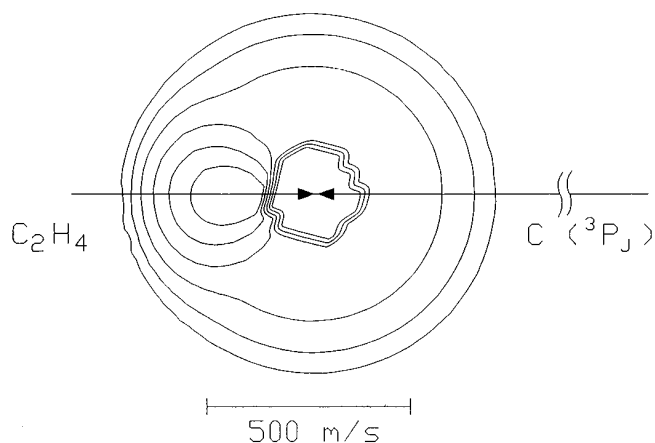

FIG. 10. Contour flux map distribution for the reaction $C(^3P_j)+C_2H_4(X\ ^1A_g)$ at a collision energy of 38.3 kJ mol^{-1}.

A. C$_3$H$_4$ *ab initio* potential energy surface

We investigate two mechanisms, the addition of $C(^3P_j)$ to the ethylenic π-bond vs insertion into the olefinic C–H bond, as well as the fate of the initially formed triplet C$_3$H$_4$ intermediates. Addition of $C(^3P_j)$ to the ethylene π-bond yields cyclopropylidene, Fig. 11, followed by ring opening to allene, or 1,2-hydrogen migration to cyclopropene. A 1,3-diradical tricarbon chain holds no local minimum on the triplet C$_3$H$_4$ PES. Triplet-allene fragments via C–H bond cleavage to the propargyl radical or undergoes 1,2-H-migration to triplet *trans/cis* vinylmethylene or 1,3-H-migration to triplet methylacetylene, which subsequently yields propargyl or propyn-1-y1 via C–H bond rupture. Triplet cyclopropene either decomposes to cyclopropen-1-yl/cyclopropen-2-yl radicals, or ring opens to vinylmethylene. This might fragment to the propargyl radical. C–H bond rupture in cyclopropylidene may yield cyclopropen-2-yl. Finally, insertion of $C(^3P_j)$ into the olefinic C–H bond leads to vinylmethylene.

The rigorous identification of the propargyl radical alone eliminates all exit channels to competing C$_3$H$_3$ isomers. The

TABLE V. Minimum rotational energy E_{rot} of the propargyl radical for $K=0$, remaining vibrational energy E_{vib}, the highest energetically accessible K-states for $E_{vib}=0$, and the minimum tilt angle α_{min} of the propargyl principal axis with respect to $\mathbf{j}'$. The partitions of the total available energy in percent for $K=0$ are included in parentheses.

	$E_{coll}=17.1$ kJ mol^{-1}	$E_{coll}=38.3$ kJ mol^{-1}
E_{tot}, kJ mol^{-1}	232	253
E_{tr}, kJ mol^{-1}	71(31)	105(41)
E_{rot} ($K=0$, microchannel 2), kJ mol^{-1}	23(10)	39(15)
E_{rot} ($K=0$, microchannel 2; $K=J$, microchannel 1), kJ mol^{-1}	105(45)	127(50)
E_{vib} ($K=0$, microchannel 2), kJ mol^{-1}	138(59)	109(43)
E_{vib} ($K=0$, microchannel 2; $K=J$, microchannel 1), kJ mol^{-1}	55(24)	20 (8)
K_{max}	36	32
α_{min}	63	72

participation of a cyclopropene complex can be ruled out as well. A potential barrier connecting cyclopropylidene with cyclopropene is located at least 120 kJmol^{-1} above the transition state to allene. If a triplet cyclopropylidene complex is initially formed, the reaction proceeds via the lowest energy pathway, in our case to allene. In this framework, the large potential energy difference of both transition states and the participation of only one isomer at $m/e=39$ is consistent with the TOFs and both LAB distributions, cf. Secs. IV A–IV D. The four remaining pathways differ by the migration of a H atom before the final bond rupture, but cannot be reduced further by investigating solely the C$_3$H$_4$ PES. However, hydrogen rearrangement prior to decomposition might be involved to certain extend.

B. Rotation axis of decomposing C$_3$H$_4$ complexes

The rotational motions of the prevailing C$_3$H$_4$ complexes are very interesting and help to explain the shapes of both $T(\theta)$s, if the distributions for distinct rotations are compared to what is found experimentally. We point out that the initial trajectory of the carbon atom prior to capture is unimportant in the frame of the capture theory, since the potential energy is assumed to depend only on the C_6 parameter. But sterical effects and attractive chemical forces come into play if the capture radius is in the order of the bond lengths, so that certain approach geometries and rotations might be favored. Based on this, we identify allowed rotations in each C$_3$H$_4$ intermediate, elucidate trajectories under highest possible symmetry of $C(^3P_j)$ toward C$_2$H$_4$ which excite these rotations, and discuss the range of contributing impact parameters. Finally, we demonstrate that the title reaction proceeds via addition to the ethylene π-bond yielding cyclopropylidene, followed by ring opening to allene and decomposition to propargyl and atomic hydrogen.

1. Triplet allene complex

Maintaining the C–C–C plane as a plane of symmetry, the carbon atom might add to the C$_2$H$_4$ molecular plane conserving C_s symmetry (Fig. 12). This pathway does not force

TABLE VI. Principal moments of inertia I_i, in amu Å^2, rotational constants in MHz, and asymmetry parameters κ of triplet C_3H_4 complexes (TS: transition state) calculated from geometries in Refs. 43–55.

Complex	I_A	I_B	I_C	A	B	C	κ
trans-vinylcarbene	8.8629	44.6369	53.4998	57022	11322	9446	−0.92
cis-vinylcarbene	7.3813	47.2273	54.6086	68468	10701	9254	−0.95
allene	5.3910	51.8501	57.2411	93746	9747	8829	−0.98
allene (TS)	3.3489	58.3671	61.7160	150911	8658	8188	−0.99
methylacetylene	4.7216	45.5987	50.3203	107037	11083	10043	−0.98

perpendicular approaches towards the C=C bond, but permits rather in-plane trajectories skewed with respect to the perpendicular vector. Since $\mathbf{L} \gg \mathbf{j}$, the three heavy atoms rotate in a plane roughly perpendicular to $\mathbf{L}$ around the C-axis of the prolate cyclopropylidene adduct. The successive ring opening to triplet allene conserves C_s symmetry and converts the previously out-of-plane H-atoms into the symmetry plane. This scenario opens larger impact parameters than typical C_2H_4 bond dimensions of $r(C=C)=1.325$ Å, and $r(C–H)=1.076$ Å compared to the large b-dominated opacity function with $b_{max}=3.7$ and 3.2 Å (Secs. IV D and IV E). In addition, the nearly in-plane rotation about the C-axis gives rise to extremely low K values and, therefore, a negligible $\mathbf{J}$ component about the C_2 figure axis of the triplet allene. This rotation axis could be associated with preferentially low K states populated in the propargyl product. Therefore, our results suggest that C-like rotations of the triplet allene complex contribute predominantly to the isotropic microchannel 2, and that any of the four hydrogen atoms $H1$–$H4$ departs with almost equal probability to yield a weak $\mathbf{L}$-$\mathbf{L}'$ correlation. Alternatively, a long-lived complex behavior was suggested in Sec. IV D, but can likely be dismissed: The rising collision energy should reduce the lifetime of the triplet allene complex and would have resulted in a more forward scattered fraction which was not verified in our experiments.

In addition, a parallel approach of $C(^3P_j)$ with respect to the ethylene plane under C_s symmetry induces rotations around the cyclopropylidene A-axis, Figs. 12 and 13. Ring opening yields triplet allene. The rotation period τ_{rot} of the complex around its A-axis helps us to elucidate the effect of these trajectories on the $T(\theta)$s. Investigating a rotation around the i-axis, τ_{rot} is calculated via Eq. (17)

$$\tau_{rot} = 2\pi I_i / L_{max} \tag{17}$$

with the moment of inertia I_i in respect to the i-axis and the maximum angular momentum L_{max}. Table 7 compiles the calculated rotational periods around the A, B, and C-axis of

TABLE VII. Rotational periods τ_{rot} of triplet allene calculated for rotations about the A, B, and C axis at collision energy E_{coll}. L_{max} denotes the maximum impact parameter.

E_{coll}, kJ mol^{-1}	I	L_{max}, $\hbar$	$\tau_{rot}(A)$, ps	$\tau_{rot}(B)$, ps	$\tau_{rot}(C)$, ps
16.1	1.7	99	0.05	0.52	0.57
38.3	2.0	128	0.04	0.40	0.44

the triplet allene complex. The rotational period depends strongly on the rotational axis A vs C and varies between 0.04 and 0.57 ps. Reactions with collision times <0.1 ps follow direct reactive scattering dynamics with almost zero intensity at $\theta=180°$.[61] Based on this and a strong $\mathbf{L}$-$\mathbf{L}'$ correlation, only A-like rotations and H2-C3/H3-C1 bond ruptures should contribute to the forward-peaked microchannel 1. This conclusion is consistent with the partition of energy into the rotational degrees of freedom and the total conservation of energy (Table V), calculated for a dominant end-over-end rotation of propargyl (microchannel 2) and contributions of 8%–14% A-like rotations (microchannel 1). However, a rapid inversion of triplet allene via a planar, D_{2h} transition state (Fig. 13) could induce a symmetric exit transition state as well as $T(\theta)$ and could contradict our findings. Although the inversion barrier height ranges about 25 kJmol^{-1}, well below the total available energy, the transition state would rotate fast about its principal axis with $K\approx J$. This increases the inversion barrier to at least 420 kJmol^{-1} at $E_{coll}=17.1$ kJmol^{-1} and 650 kJmol^{-1} at $E_{coll}=38.3$ kJmol^{-1}, well above the total available energy. Bulk experiments support our conclusion of dominating C-rotations. The typical time between two collisions of the initially formed C_3H_4 complex in ^{11}C tracer studies and a second bath molecule are on the order of 1 ps at 100 Torr neat ethylene. A lifetime at least one order of magnitude less cannot account for detected $C5$ compounds.

Finally, we discuss the potential contribution of B-type rotations of the triplet allene complex (Fig. 13). B-transitions can be excited by C-atom trajectories following C_1 symmetry and give rise to a symmetric exit transition state, since $H2$ and $H3$ as well as $H4$ and $H1$ can depart from either end, cf. Sec. IV D. Therefore, the strongly forward scattered microchannel 2 can be dismissed. Based only on the experimentally found $T(\theta)$, a symmetric transition state might explain microchannel 2. Compared to reactions conserving C_s symmetry, however, encounters without any symmetry element show a reduced overlap of the p-type orbitals of the C-atom with the π-molecular orbital of the ethylene molecule, and should be energetically less favorable.

2. Triplet cis/trans vinylcarbene complex

A pathway to triplet *cis/trans* vinylcarbene follows either 1,2-H-migration in triplet allene or a direct insertion of $C(^3P_j)$ into a C–H bond of ethylene. Figure 13 displays the principal rotational axis with the embodied carbon atom designated as $C2$ and $C3$, respectively. As evident, only a
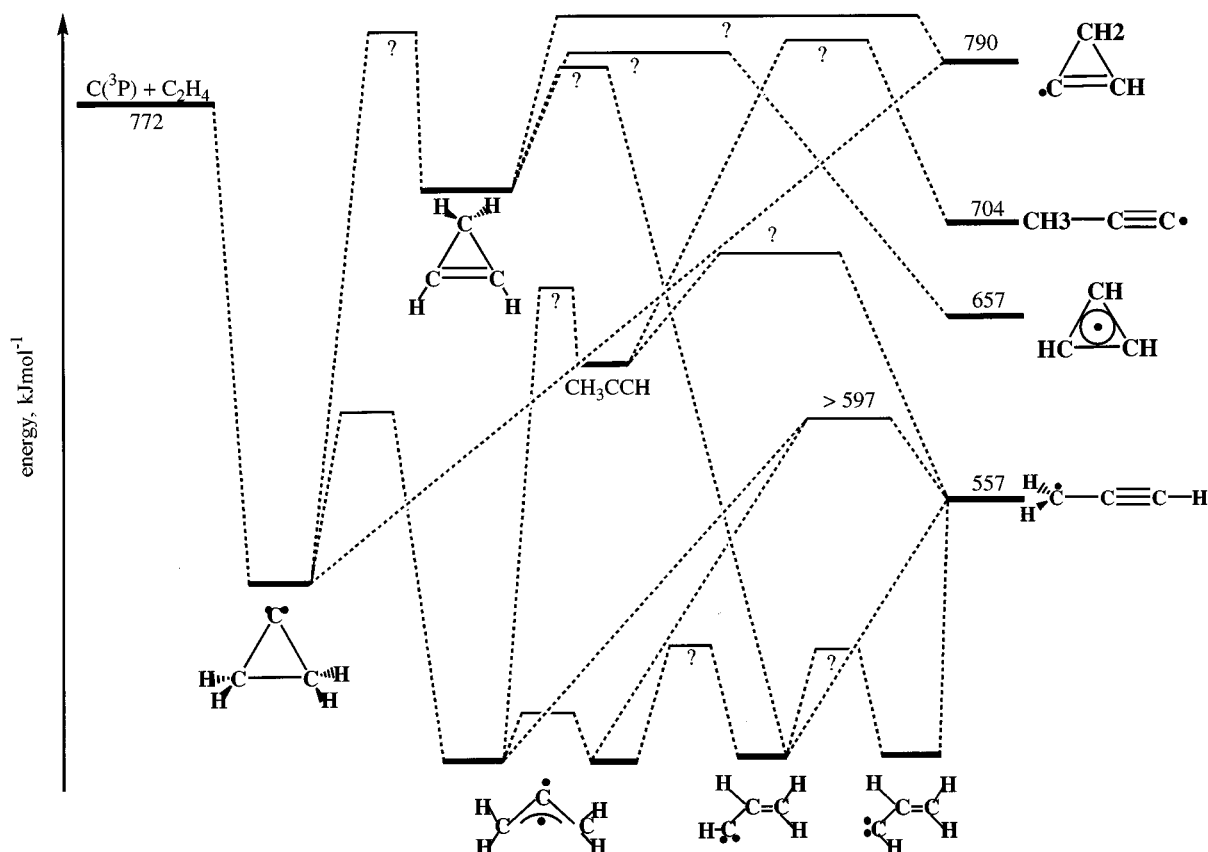
FIG. 11. Schematic representation of the lowest energy pathways on the triplet C_3H_4 PES and structure of potentially involved collision complexes. Enthalpies of formation, electronic states, and were taken from Refs. 43–58: Cyclopropylidene (1): 501 kJ mol^{-1}, $^3B_1$, C_{2v}; allene (2/2'): 405 kJ mol^{-1}, $^3A_2$, C_{2v}; cyclopropene (3): ~720 kJ mol^{-1}; propargyl (4): 557 kJ mol^{-1}, $^2B_2$, C_{2v}; cis vinylcarbene (5): 408 kJ mol^{-1}, $^3A''$, C_s; trans vinylcarbene (6): 409 kJ mol^{-1}, $^3A''$, C_s; methylacetylene (7): ~630 kJ mol^{-1}; propyn-1-yl (8): 704 kJ mol^{-1}, ^2E, D_{3h}; cyclopropen-1-yl (9): 657 kJ mol^{-1}, $^2E''$, D_{3h}; cyclopropen-2-yl (10): 790 kJ mol^{-1}, $^2A'$, C_s ···?: No information available.

H2/C2 bond rupture in vinylcarbene yields the propargyl radical. Since any of the four hydrogen atoms is required to depart equally likely under weak **L** and **L**′ coupling to account for the isotropy of microchannel 2 (Sec. IV C), a contribution of a cis/trans vinylcarbene intermediate to microchannel 2 can be likely ruled out. Further, only A-like rotations could give rise to microchannel one. The vinylcarbene complex rotating around the B/C axis must hold lifetimes of at least 0.4–0.3 ps to induce any forward-scattering, but the strongly forward-scattered $T(\theta)$ at higher collision energy requires collision times <0.1 ps to account for a strong **L**-**L**′ correlation.[61] These rotations around the A-axis are induced, if $C(^3P_j)$ inserts via a perpendicular pathway into the C–H bond of the ethylene molecule. This trajectory, however, seems unlikely, since only a narrow range of impact parameters between 0.66 and 1.2 Å contributes to reactive scattering signal. The overwhelming contribution of large impact parameters up to 3.7 Å was already validated. Likewise, this insertion resembles a symmetry forbidden reaction, and an entrance barrier larger than our maximum collision energy of 38.3 kJmol^{-1} is expected. Our interpretation correlates with ^{11}C-tracer experiments: thermal $^{11}C(^3P_j)$ and

even $^{11}C(^1D_2)$ add to the π-bond, but only suprathermal C-atoms in both spin states insert into the C–H bond. The only remaining pathway to A-like rotations in vinylcarbene involves a [3,2]-H-shift in triplet allene, rotating around its A-axis. Since the forward-peaking demands collision times
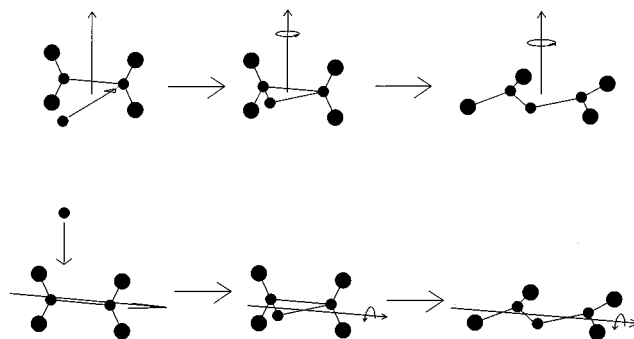

FIG. 12. Approach geometries of the carbon atom toward the ethylene molecule conserving C_s symmetry and induced rotations. Upper: Perpendicular approach; lower: Parallel approach.
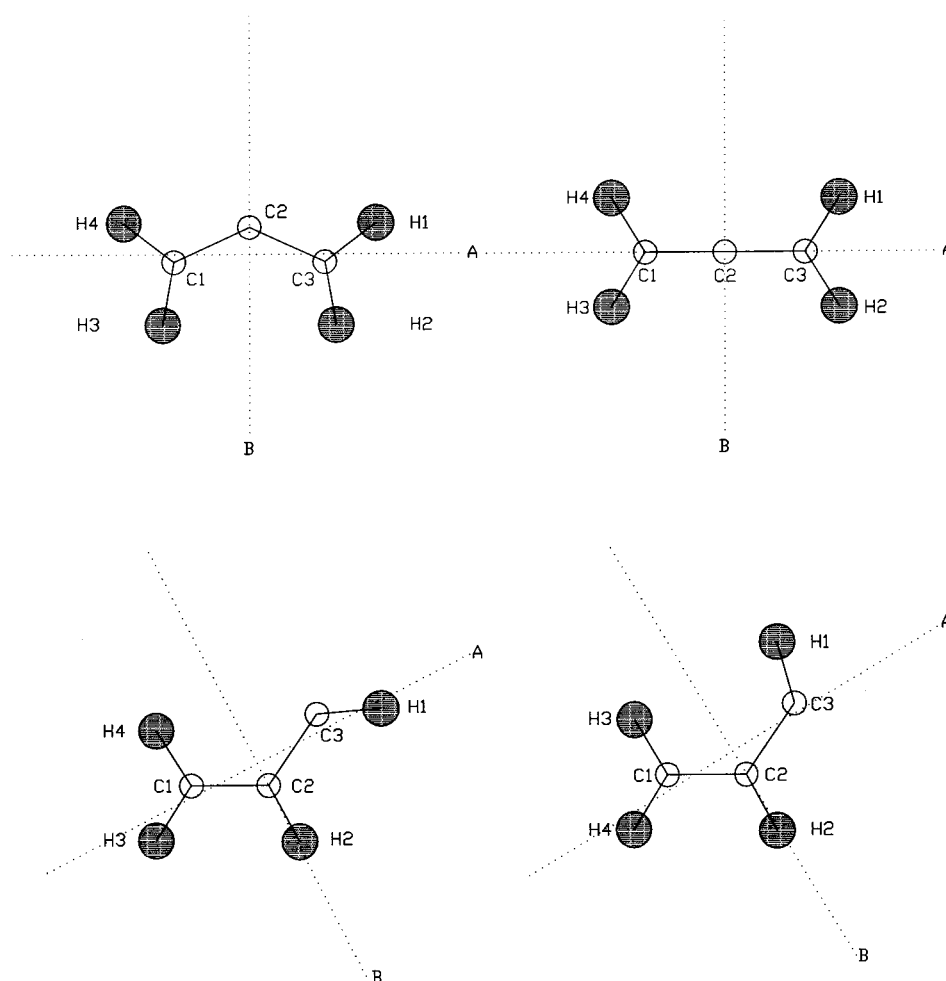
FIG. 13. Rotation axis of triplet C_3H_4 isomers calculated with moments of inertia of Table VI; the C axis is perpendicular to the paper plane. Hydrogen atoms are hatched. The designation is taken from Fig. 11. Top left: allene; top right: TS of allene inversion; bottom left: *cis* vinylcarbene; bottom right: *trans* vinylcarbene.

<0.1 ps, a hydrogen migration can most likely be excluded. Even a fast $[1,2]$-H-rearrangement from vinylidene to acetylene takes more than 0.2 ps.[62]

3. Triplet methylacetylene complex

The triplet allene-methylacetylene rearrangement involves a symmetry-allowed $[1,3]$-H-shift[60] similar to Sec. V B. The height of this barrier, however, ranges well above any conceivable one arising from $[1,2]$-H-migration. Considering that the lower energy pathway is closed, $[1,3]$-H-migration cannot take place either.

C. Surface splitting

The symmetry of the total wave function has to be conserved during the title reaction and is assumed to be separable into an electronic and spin part. Since we are dealing with light carbon atoms and the spin–orbit coupling constant increases with the fourth power of the nuclear charge, this simplification is justified. Interacting under highest possible C_s symmetry, the P-term of the carbon atom splits into the irreducible representations $A''+A''+A'$. The C_2H_4 symme-

try reduces to A'. The total electronic wave function is gained via the direct product of the reactant's wave function

$$(A''+A''+A')\times A'=2A''+A'. \tag{18}$$

The B_2 ground state of the propargyl radical reduces to A'' in C_s symmetry (C-like rotations of the triplet allene complex) and the S state of hydrogen atom to A'

$$A''\times A'=A''. \tag{19}$$

The ground state electronic wave functions of all triplet complexes and transition states involved in the elucidated reaction pathway, i.e., cyclopropylidene and allene, belonging to the A'' representation. Therefore, reactants, collision complexes, and products correlate on the A'' surface, and the title reaction can proceed on the A'' ground state surface under C_s symmetry via excitation of C-like rotations. If the carbon atom approaches slightly off-axis, the C_s symmetry reduces to C_1 and the electronic wave function to A. Likewise, A-rotations of the decomposing triplet allene complex do not conserve the symmetry plane in the final carbon-hydrogen bond rupture, and the symmetry of the electronic wave func-
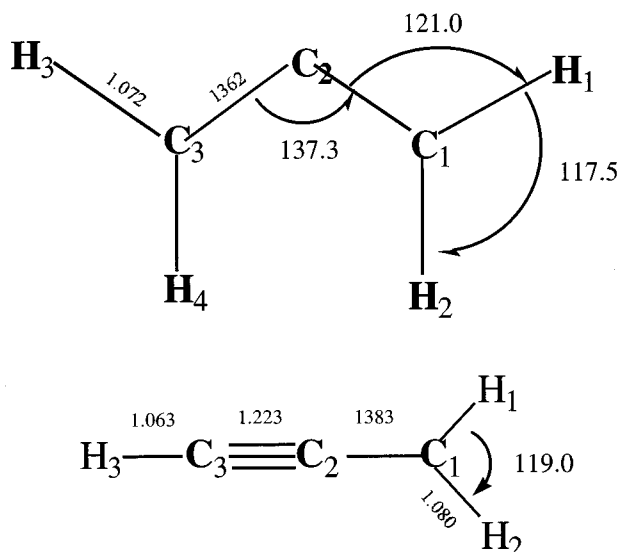
FIG. 14. Equilibrium geometries of triplet allene and the propargyl radical Refs. 36–37.

tion is reduced to ^3A. Finally, we point out that the opacity function $P(b)$ might be different for the ^3A (microchannel 1) and $^3A''$ surface (microchannel 2). This could account for the deviation of the relative energy dependent cross sections from the simple capture picture as well.

D. Exit transition state

The collision energy dependent $P(E_T)$ shape and their average translational energy releases, $\langle E_T \rangle$ reveal the chemical dynamics between the moment of the triplet allene complex formation and the final separation into products. As shown in Sec. IV C, both $P(E_T)s$ peak at 28–43 kJmol^{-1} and indicate that the C–H bond rupture in triplet allene does not resemble a system with a loose transition state. This finding and the lack of intensity in both $P(E_T)s$ below 3 and 12 kJmol^{-1} suggest instead a tight transition state, and should go hand in hand with a significant geometry change from the triplet allene complex to the propargyl radical. As evident from Fig. 14, this requirement is fulfilled. Predominantly, the $C2$-$C3$-bond length in the propargyl radical is reduced by 0.141 Å, corresponding to a bond order increase from 1.5 to 3, and the $C1$-$C2$-$C3$ bond angle widens by 52.7°. The order of magnitude of the exit barrier is consistent when compared to the 7–10 kJmol^{-1} peaking $P(E_T)$ of the reaction C(^3P_j)+C$_2$H$_2$ $(X^1\Sigma_g^+)\rightarrow$1–C$_3$H+H:[63] The carbon chain is almost linear in the triplet propargylene complex, HCCCH, as well as in the 1-C$_3$H product, and the internuclear distances differ by less than 0.05 Å. But even the tight transition state theory of Marcus predicts an increasing fraction of total available energy channeling into vibration as the collision energy rises, if the energy is completely randomized.[64] Therefore, our decrease of fractional vibrational energy deposition as the collision energy rises (Sec. VI F) suggests an incomplete energy randomization in the

triplet allene complex prior to decomposition. Hence, the lifetime of the triplet C$_3$H$_4$ complex is too short.

E. Possible contributions from the singlet C$_3$H$_4$ surface

The experimental results strongly indicate that the title reaction proceeds on the ground-state triplet surface. However, we will also investigate the singlet PES for completeness. Here, intersystem crossing (ISC) might occur if the spin–orbit coupling operator acts as a perturbation capable of mixing the triplet wave function ($^3B_2$ in cyclopropylidene, $^3A_2$ in allene) with the final singlet wave function ($^1A_1$ in cyclopropylidene and allene; reduced via C_{2v} symmetry). Since the operators transform as rotations, they span the irreducible representations A_2, B_1, and B_2. Hence, the a^3B_2 state of cyclopropylidene is mixed via a B_2 spin–orbit operator with X^1A_1 and the allene a^3A_2 state via a A_2 operator to its electronic ground state. This direct product approach however, yields no information on the magnitude of the spin–orbit interaction. Since no heavy atom is present in our complexes and the spin–orbit coupling constant rises with the fourth power of the atomic number, the ISC crossing is too slow compared to the lifetime τ of the C$_3$H$_4$ complex. This conclusion is consistent when comparing the rotational period of the triplet allene complex with typical ISC timescales: Even the largest known ISC rate constants between $10^{10}-10^{11}$ s^{-1} for polycyclic aromats containing heavy atoms, e.g., bromonaphthalene, are at least one order of magnitude too low.[65]

An alternative ISC mechanism follows a rotation of two perpendicular π-electron systems each filled with one electron.[66–67] In the case of triplet cyclopropylidene as well as allene, the first electron occupies a π-type orbital, the second one a nonbonding orbital with σ-symmetry. Therefore, this pathway cannot contribute to ISC in the title reaction. Summarized, our findings indicate ISC should not play an important role and strongly correlate with ^{11}C($^3P_j/^1D_2$) tracer experiments in C$_2$H$_4$ systems: allene molecules are solely the reaction product of C($^1D_2$) with a single ethylene molecule. C(^3P_j) yields triplet C$_3$H$_4$ which fragments or reacts with a second C$_2$H$_4$ molecule.

F. Comparison with the reaction O(^3P_j)+C$_2$H$_4$

The dynamics of the reaction O(^3P_j) with C$_2$H$_4$ were recently studied in our lab[28] and two major channels were detected. The oxygen–hydrogen exchange channel yields H+C$_2$H$_3$O on the $^3A''$ surface via a short lived triplet 1,3 CH$_2$CH$_2$O diradical undergoing C–H bond rupture. Alternatively, the C$_2$H$_4$O complex undergoes ISC, followed by 1,2-hydrogen migration to acetaldyhyde and C–C bond rupture to CH$_3$ and HCO. The different dynamical behavior as compared to C(^3P_j)+C$_2$H$_4$ is solely the effect of a stable triplet-1,3-diradical on the C$_2$H$_4$O PES and a successive ISC via rotation of both perpendicular π-electron systems to a deep potential well. These dynamics increase the lifetime of the complex and open up the channel of H-migration to acetaldehyde. A triplet, 1,3 CH$_2$CH$_2$C diradical, however, holds no

local minimum on the C_3H_4 PES and collapses to cyclopropylidene. ISC, successive ring opening to allene, and 1,2-H-migration to singlet methylacetylene are closed, and no CH_3-loss can occur.

G. Undetected channels

The dynamics of the title reaction account for the unobserved exothermic exit channels (Table II). First, all singlet channels 6, 8, and 9 to C_3H_2-isomers as well as to CH_4, # 19, are closed, since the reaction proceeds via spin conservation on the triplet surface. Reactions (10) and (11) to triplet cyclopropenylidene and vinylidenecarbene must proceed via cyclopropylidene and allene, respectively. Channel 10 is a symmetry-forbidden, 4 center-4 electron elimination (retro-addition of H_2 to the C=C in triplet cyclopropenylidene), whereas # 11 involves a symmetry forbidden, 3 center-4 electron elimination (retro cheletop reaction of H_2 with vinylidenecarbene). Both pathways are expected to involve a symmetry imposed barrier: lower barrier limits of 82 kJmol^{-1} (# 10) and 103 kJmol^{-1} (# 11) are reasonable for this class of symmetry forbidden reactions.[68] Reaction to triplet propargylene (# 7) must pass triplet allene, but geometrical constraints hinder this pathway. Further, elimination of a CH_3 group (# 18) remains unobserved, and the 1,3-H-migration to triplet methylacetylene is likely prevented in the triplet allene complex.

Channel 17 remains the only additional pathway. However, a direct fragmentation of cyclopropylidene or allene to C_2H_2 is not feasible. The elimination must proceed via a cyclopropylidene ring cleavage [retrocycloaddition of $CH_2(X^3B_2)$ to H_2CC, vinylcarbene (X^1A_1)] or a C1-C2 bond cleavage in allene to $CH_2(X^3B_2) + H_2CC$ (X^1A_1). Since vinylcarbene ranges ~ 180 kJmol^{-1} higher in energy than acetylene and the 1,2-H-migration to C_2H_2 involves a barrier of about 11 kJmol^{-1}, the transition state is placed about 30 kJmol^{-1} above the reactants. Hence, channel 18 could only be opened at the higher collision energy of 38.3 kJmol^{-1} and might explain the deviation of the experimentally determined cross-section ratio from the theoretical one, cf. Sec. IV E as well as the diminishing acetylene yield in ^{11}C tracer experiments with increasing thermalization.

### VI. IMPLICATIONS TO INTERSTELLAR CHEMISTRY AND COMBUSTION PROCESSES

The explicit identification of the C_3H_3 propargyl isomer in the crossed beam reaction $C(^3P_j)$ with C_2H_4 portrays a further example of the dominant carbon–hydrogen exchange channel in the reaction of neutral carbon atoms with unsaturated hydrocarbons.[63] This pathway was elucidated recently based on molecular beams studies of reaction (20)

$$C(^3P_j) + C_2H_2(X\ ^1\Sigma_g^+) \rightarrow C_3H + H, \tag{20}$$

and presents an alternative, one-step approach to build up carbon bearing molecules in interstellar environments and hydrocarbon flames. Competing ion-molecule reactions (21–23), for example,

$$C_2H_4 + C^+ \rightarrow c - C_3H_3^+ + H, \tag{21}$$
$$\rightarrow c - C_3H_2^+ + H_2, \tag{22}$$
$$\rightarrow l - C_3H_2^+ + H_2, \tag{23}$$
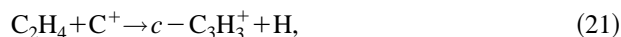
hold higher rate constants with $k(C^+ + C_2H_4;\ 293$ K)$ = (1.2\pm0.1)\times10^{-9}$ cm^3 s^{-1} as compared to the atom neutral reaction $k(C + C_2H_4;\ 293$ K)$ = (2.0\pm0.1)\times10^{-10}$ cm^3 s^{-1}, but modeling of high and low ionization phases in dark interstellar clouds yielded neutral carbon fractional abundances of about 10^{-5} and 10^{-7} vs C^+ data of $\sim3\times10^{-8}$ and 3×10^{-9}, respectively.[69] White and Sandell[70] confirmed these calculations and observed neutral carbon fractional abundances between 3.0×10^{-5} and 5.0×10^{-7} toward OMC-1. These data clearly undermine the order-of-magnitude advantage for the rate of ion-molecule reactions as compared to atom-molecule reactions. Most important, however, synthesis of carbon-hydride radicals via atom-neutral reaction proceeds in one step, eliminating the need for successive binary encounters. Lowest applied translational energies of ~17.1 kJmol^{-1} in our experiments are equivalent to about 1500 K and are easily accessible in the outflow of carbon stars with temperatures up to 4000 K. In addition, a verified rising reactive cross sections with decreasing collision energy identifies this reaction class as a potentially important means to form complex hydrocarbons even for dark and diffuse interstellar clouds, but extrapolation to typical temperatures of 10–100 K depends on the absence of small entrance barriers. Our findings, however, strongly encourage astronomical search for the hitherto unobserved propargyl isomer and hydrocarbon radicals as potential C–H exchange channels of atom-neutral reactions, e.g.,

$$C(^3P_j) + HCCCH_3 \rightarrow C_4H_3 + H. \tag{24}$$
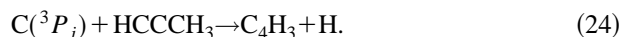
In particular, methylacetylene has been widely observed toward the Orion ridge and TMC-1. These clouds serve as ideal targets to identify potential C_4H_3-isomers, perhaps among unidentified microwave transitions in the spectrum toward OMC-1.

VII. CONCLUSIONS

The reaction between ground state carbon atoms, $C(^3P_j)$, and ethylene, $C_2H_4(X^1A_g)$, was studied at average collision energies of 17.1 and 38.3 kJmol^{-1} using the crossed molecular beam technique. Our results suggest two microchannels, both initiated via an attack of the carbon atom to the π-orbital of the C_2H_4 molecule via a loose, reactant like transition state located at the centrifugal barrier. One microchannel follows the highest symmetric C-atom approach via C_s symmetry on the ground state $^3A''$ surface and contributes to an isotropic center-of-mass angular distribution. Initially, the cyclopropylidene complex rotates in a plane roughly perpendicular to $\mathbf{J}$ around its C-axis and undergoes ring opening to allene prior to decomposition to the propargyl radical in its X^2B_2 state. A second microchannel contributes $\sim10\%$ of the scattering signal. Here, the A-like rotations of the cyclopropylidene adduct, ring opening to triplet allene, and a

strong $\mathbf{L}$-$\mathbf{L}'$ correlation give rise to a forward-peaking $T(\theta)$. Both exit transition states are found to be tight and located at least 30–40 kJmol^{-1} above the products.

This mechanism is consistent with ^{11}C(^3P_j)-tracer studies under bulk conditions. The postulated triplet cyclopropylidene complex was trapped as a spirane, and an assumed C_3H_3 intermediate yielded 1-propyneyl-5 and 1,2-pentadienyl-5 products. The acetylene production can be explained by assuming a second, but in our experiments undetected channel of the allene complex decomposing to vinylidene and triplet carbene.

The explicit identification of C_3H_3 under single collision represents a second example of a carbon–hydrogen exchange in reactions of ground-state carbon with unsaturated hydrocarbons. This versatile concept represents an alternative pathway to build up unsaturated hydrocarbons chains in combustion processes and in the interstellar medium.

Note added in proof. The assignment of the symmetry of the electronic wave function for C_{2v} molecules follows the convention that the molecular plane is defined as the mirror plane, e.g., $C_3H_3(X^2B_2)$ instead of $C_3H_3(X^2B_1)$.

ACKNOWLEDGMENTS

APPENDIX

The total energy of the system E_T [Eq. (A1)] is the sum of the kinetic energy of the reactants (A2) with the reduced mass μ at distance R and the effective potential $V_{\text{eff}}(R)$ as a sum of a repulsive centrifugal potential $V_{\text{cen}}(R)$ Eq. (A3) and an attractive intermolecular dispersion term $V_{\text{disp}}(R)$ with the Lennard-Jones-coefficient C_6 [Eq. (A4)]

$$E_T = E_{\text{kin}}(R) + V_{\text{eff}}(R) = E_{\text{kin}}(R) + V_{\text{cen}}(R) + V_{\text{disp}}(R), \tag{A1}$$

$$E_{\text{kin}} = \tfrac{1}{2}\,\mu\dot{R}^2, \tag{A2}$$

$$V_{\text{cen}}(R) = \frac{E_T b^2}{R^2}, \tag{A3}$$

$$V_{\text{disp}}(R) = -\frac{C_6}{R^6}. \tag{A4}$$

The effective potential holds a maximum at $R = R_{\text{max}}$ [Eq. (A5)] giving rise to the barrier location at R_{max} [Eq. (A6)]; if the reactant approaches within R_{max}, chemical forces take over.

$$\left[\frac{dV_{\text{eff}}(R)}{dR}\right]_{R=R_{\text{max}}} = 0, \tag{A5}$$

$$R_{\text{max}} = (6\mu C_6/L^2)^{1/4}. \tag{A6}$$

Consequently, the remaining kinetic energy at $R \leqslant R_{\text{max}}$ has to fulfill the condition for reaction

$$\frac{1}{2}\,\mu\dot{R}^2 = \left[E_T - \frac{E_T b^2}{R^2} + \frac{C_6}{R^6}\right]_{R=R_{\text{max}}} \geqslant 0, \tag{A7}$$

yielding the maximum impact parameter b_{max}

$$b_{\text{max}} = \left[\frac{L_{\text{max}}^2}{2\mu E}\right]^{1/2}. \tag{A8}$$

This treatment assumes the reaction proceeds with unit efficiency after barrier-crossing and under absence of sterical effects. The Lennard-Jones coefficient C_6 is approximated according to Hirschfelder *et al.*[71] to

$$C_6 = \frac{3}{2}\left(\frac{E_C E_{C2H4}}{E_C + E_{C2H4}}\right)\alpha_C \alpha_{C2H4}, \tag{A9}$$

with the ionization potentials E_i for $i = C(^3P_j)$, and $C_2H_4(X\ ^1A_g)$, and the polarizabilities α_i. Using $\alpha_{C(3pj)} = 1.76 \times 10^{-30}$ m^3, $\alpha_{C2H4} = 4.25 \times 10^{-30}$ m^3, $E_{C(3Pj)} = 11.76$, $E_{C2H4} = 10.5$ eV, the maximum impact parameter b_{max} calculates to b_{max} (17.1 kJmol^{-1}) = 3.7 Å and b_{max} (38.3 kJmol^{-1}) = 3.2 Å (Table II).

[1] E. Herbst, H. H. Lee, D. A. Howe, and T. J. Millar, Mon. Not. Royal Astronomical Society **268**, 335 (1994).
[2] *Symposium on Titan* (ESA-SP 338, ESTEC, Noordwijk, 1992).
[3] R. D. Kern, K. Xie, and H. Chen, Combust. Sci. and Tech. **85**, 77 (1992).
[4] G. J. Collin, H. Deslauriers, G. R. De Mare, and R. A. Poirier, J. Phys. Chem. **94**, 134 (1990).
[5] P. R. Westmoreland, A. M. Dean, J. B. Howard, and J. P. Longwell, J. Phys. Chem. **93**, 8171 (1989), and references therein.
[6] G. Rotzell, Int. J. Chem. Kinetics **17**, 637 (1985).
[7] R. D. Smith, Combust. Flame **35**, 179 (1979).
[8] I. R. Slagle and D. Gutman, Proc. 23rd Symp. Int. Combust. Chemistry, 875 (1988).
[9] J. A. Miller and C. F. Melius, Combustion and Flame **91**, 21 (1992).
[10] J. D. Adamson, C. L. Morter, J. D. DeSain, G. P. Glass, and R. F. Curl, J. Phys. Chem. **100**, 2125 (1996).
[11] L. R. Thorne, M. C. Branch, D. W. Chandler, R. J. Kee, and J. Miller, Proc. 21st Symp. Int. Combust. Chemistry, 965 (1986).
[12] D. Toublanc, J. P. Parisot, J. Brillet, D. Gautier, F. Raulin, and C. P. McKay, Icarus **113**, 2 (1995).
[13] Y. H. Kim and J. L. Fox, Icarus **112**, 310 (1994).
[14] E. Herbst, Angew. Chemie **102**, 627 (1990).
[15] E. Herbst and C. M. Leung, Ap. J. Supl. Ser. **69**, 271 (1989).
[16] M. Marshall, C. MacKay, and R. Wolfgang, J. Am. Chem. Soc. **86**, 4741 (1964).
[17] G. Stoecklin, *Chemie heisser Atome* (Weinheim, VCH, 1969).
[18] A. P. Wolf, in *Hot Atom Chemistry Status Report* (IAEA, Vienna, 1975), pp. 203–209.
[19] C. MacKay, J. Am. Chem. Soc. **83**, 2399 (1961).
[20] P. Gaspar, in *Handbook of Hot Atom Chemistry*, edited by J.-P. Adloff, P. P. Gaspar, M. Imamura, A. G. Maddock, T. Matsuura, H. Sano, K. Yoshihara (VCH, Weinheim, 1992).
[21] J. Dubrin, C. MacKay, and R. Wolfgang, J. Am. Chem. Soc. **86**, 959 (1964).
[22] J. Dubrin, H. Rosenberg, R. Wolfgang, and C. MacKay, in *Chemical Effects of Nuclear Transformations* (Elsevier, New York, 1979), p. 238.
[23] J. Nicholas, C. MacKay, and R. Wolfgang, Tetrahedron **22**, 2967 (1966).
[24] M. Marshall, Ph.D. thesis, Yale University, 1969.
[25] F. F. Martinotti, M. J. Welch, and A. P. Wolf, J. Chem. Soc. D, 115 (1968).
[26] *Handbook of Chemistry and Physics* (CRC Press, Boca Raton, 1995).
[27] Y. T. Lee, Science **236**, 793 (1987).
[28] A. M. Schmoltner, P. M. Chu, R. J. Brudzynski, and Y. T. Lee, J. Chem. Phys. **91**, 6926 (1989).

[29] Y. T. Lee, J. D. McDonald, P. R. LeBreton, and D. R. Herschbach, Rev. Sci. Instr **40**, 1402 (1969).

[30] R. I. Kaiser and A. G. Suits, Rev. Sci. Instr. **66**, 5405 (1995).

[31] G. O. Brink, Rev. Sci. Instr. **37**, 857 (1966).

[32] N. R. Daly, Rev. Sci. Instr. **31**, 264 (1960).

[33] J. M. Parson, K. Shobatake, Y. T. Lee, and S. A. Rice, J. Chem. Phys. **59**, 1402 (1973).

[34] M. S. Weis, Ph.D. thesis, University of California, Berkeley, 1986.

[35] M. Vernon, Thesis, University of California, Berkeley, 1981.

[36] R. Herges and A. Mebel, J. Am. Chem. Soc. **116**, 8229 (1994).

[37] S. Walsh, NASA Ames Research Center, Moffet Field (private communication).

[38] R. I. Kaiser, Y. T. Lee, and A. G. Suits, J. Chem. Phys. (submitted).

[39] A deviation of this long-lived complex outcome occurs, if a long-lived complex decomposes with oblate symmetry and energy conservation excludes states with high M' values (M': Projection of the total angular momentum vector $\mathbf{J}$ on the relative velocity vector of the departing fragments, $\mathbf{v}'$). In this scenario, the $T(\theta)$ maximum shifts from 90° to an intermediate position.

[40] W. B. Miller, S. A. Safron, and D. R. Herschbach, Discuss. Faraday. Society **44**, 108, 291 (1967).

[41] W. B. Miller, Ph.D. thesis, Harvard University, Cambridge, 1969.

[42] D. C. Clary, N. Haider, D. Husain, and M. Kabir, Ap. J. **422**, 416 (1994).

[43] P. Botschwina, R. Oswald, and J. Flügge, Z. Phys. Chemie **188**, 29 (1995).

[44] C. J. Cramer and S. E. Worthington, J. Phys. Chem. **99**, 1462 (1995).

[45] M. Monnier, A. Allouche, P. Verlaque, and J.-P. Aycard, J. Phys. Chem. **99**, 5977 (1995).

[46] O. A. Mosher, W. M. Flicker, and A. Kuppermann, J. Chem. Phys. **62**, 2600 (1975).

[47] W. C. Shakespeare and R. P. Johnson, J. Org. Chem. **56**, 6377 (1991).

[48] P. Warner and R. Sutherland, J. Org. Chem. **57**, 6294 (1992).

[49] C. W. Bauschlicher and S. R. Langhoff, Chem. Phys. Let. **193**, 380 (1992).

[50] A. Rauk, W. J. Bouma, and L. Radom, J. Am. Chem. Soc. **107**, 3780 (1985).

[51] D. W. Ball, R. G. S. Pong, and Z. H. Kafafi, J. Am. Chem. Soc. **115**, 2864 (1993).

[52] N. Honjou, J. Pacansky, and M. Yoshimine, J. Am. Chem. Soc. **107**, 5332 (1985).

[53] M. Yoshimine, J. Pacansky, and N. Honjpu, J. Am. Chem. Soc. **111**, 2785 (1989).

[54] R. O. Angus, M. W. Schmidt, and R. P. Johnson, J. Am. Chem. Soc. **107**, 532 (1985).

[55] S. Xantheas, S. T. Elbert, and K. Ruedenberg, Theor. Chim. Acta **78**, 365 (1991).

[56] N. Honjou, J. Pacansky, and M. Yoshimine, J. Am. Chem. Soc. **106**, 5361 (1984).

[57] P. Valtazanos, S. T. Elbert, S. Xantheas, and K. Ruedenberg, Theor. Chim. Acta **78**, 287 (1991).

[58] M. Yoshimine, J. Pacansky, and N. Honjou, J. Am. Chem. Soc. **111**, 4198 (1989).

[59] Care has to be taken to classify symmetry allowed and forbidden reactions in open shell triplet biradicals.

[60] See Ref. 59. In closed shell molecules, 1-3-H-migrations are symmetry forbidden.

[61] R. D. Levine and R. B. Bernstein, *Molecular Reaction Dynamics and Chemical Reactivity* (Oxford University Press, Oxford, 1987).

[62] T. Carrington, L. M. Hubbard, H. F. Schaefer, and W. H. Miller, J. Chem. Phys. **80**, 4347 (1981).

[63] R. I. Kaiser, Y. T. Lee, and A. G. Suits, J. Chem. Phys. **103**, 10395 (1995).

[64] R. A. Marcus, J. Chem. Phys. **62**, 1372 (1975).

[65] N. J. Turro, *Modern Molecular Photochemistry* (University Science Books, Milla Valley, 1991).

[66] K. Tanaka and M. Yoshimine, J. Am. Chem. Soc. **102**, 7566 (1980).

[67] A. P. Scott, R. H. Nobes, H. F. Schaefer, and L. Radom, J. Am. Chem. Soc. **116**, 10159 (1994).

[68] T. A. Albright, J. K. Burdett, and M. H. Whangbo, *Orbital Interactions in Chemistry* (New York, Wiley, 1985).

[69] P. Schilke, J. Keene, J. le Bourlot, J. P. Des Forets, and E. Roueff, Astronomy and Astrophysics **294**, L17 (1995).

[70] G. J. White and G. Sandell, Astronomy and Astrophysics **299**, 179 (1995).

[71] J. O. Hirschfelder, C. F. Curtiss, R. B. Bird, *Molecular Theory of Gases and Liquids* (Wiley, New York, 1954).